Oceanologia 64 (2022) 212—226

Available online at www.sciencedirect.com

ScienceDirect

journal homepage: www.journals.elsevier.com/oceanologia

ORIGINAL RESEARCH ARTICLE

Bedforms evolution in the Vistula River mouth during extreme flood event, southern Baltic Sea

Aliaksandr Lisimenka[a,b,*], **Adam Kubicki**[c], **Maciej Kałas**[a]

[a] *Maritime Institute, Gdynia Maritime University, Gdańsk, Poland*
[b] *Institute of Oceanology, Polish Academy of Sciences, Sopot, Poland*
[c] *GEO Ingenieurservice Nord-West, Wilhelmshaven, Germany*

Received 6 August 2021; accepted 20 October 2021
Available online 6 November 2021

KEYWORDS
Bedform geometry;
Bed roughness;
Flood event;
Anti-clockwise hysteresis;
Spectral analysis;
Vistula River mouth

Abstract Results of bathymetric surveys conducted to examine changes of sand dunes geometry in the Vistula River mouth before, during and after the extreme flood event are presented. A total of 2076 dunes were analysed based on a series of bed elevation profiles obtained along the centreline of about 3.3 km length. Low-steepness dunes characterized by the mean lee-side slopes milder than $\beta<10°$ are fully dominant at low flows. In contrast, at high hydrology, nearly 50% of dunes indicate $\beta>10°$. Dune height and length are substantially out of phase with progressive changes of water discharge exposing a well-pronounced anti-clockwise hysteresis. Distinct behaviour of dune dimensions reflected in increasing of dune steepness H/λ of about 3-fold and decreasing of about 4-fold were observed during rising and falling discharges, respectively. The bed roughness due to dunes presence showed changes of about 10-fold during the both of limbs and is found to be in range of about $k_{dunes}=(1/5\div3/5)H_{mean}$. At the mesoscale region, spectra followed sufficiently by the '−3 power law' for low hydrology, with steeper spectrum slopes close to '−4' during moderate and high water discharges. With the development of the flood, potential of flow separation phenomena was increased of about 9-fold, from 2.2% at the flood beginning phase up to 20% at the flood peak. The obtained results could be used for the improvement of the hydraulic numerical models in sand-bed rivers to predict bed-

* Corresponding author at: Maritime Institute, the Gdynia Maritime University, Gdańsk, Poland.
E-mail addresses: alisimenka@im.umg.edu.pl, sasha@iopan.pl (A. Lisimenka).
Peer review under the responsibility of the Institute of Oceanology of the Polish Academy of Sciences.

Production and hosting by Elsevier

https://doi.org/10.1016/j.oceano.2021.10.005

forms evolution, flow resistance and turbulence as well as water levels for proper river system management during flood events.

1. Introduction

Bedforms, such as ripples and dunes (*sensu* Ashley, 1990), are common sedimentary structures omnipresent in alluvial river channels and seabeds. They look like a series of rhythmic undulations of bed surface, typically composed of mixture of different grain sizes ranging from sands to gravels. In response to routinely changing water flow conditions observed in natural environments, these morphological elements are in ceaseless motion triggering changes in their size, shape and cross-strata structure. Bedforms are a key features for understanding of depositional/erosional processes, changes in riverine morphodynamics and sediment transport (Wu et al., 2021). They impact functioning of habitats and often present a major problem for engineering structures (Aberle et al., 2010; Amsler and Garcia, 1997).

Due to substantial influence of dunes on flow velocity structure which, in turn, impacts directly sediment transport pattern, an appreciation of the interaction between water flow, dune geometry and dune migration is therefore fundamental to predict flow resistance, bed level adjustments as well as stratification of bed sediments (Carling et al., 2000). In fact, amongst other factors like grain resistance (or roughness), vegetation one, or resistance caused by water flow field variations in space and time, the hydraulic roughness of river channels is commonly dominated by the resistance induced by subaqueous bedforms, i.e. ripples and dunes (Warmink et al., 2007, 2012, 2013). In addition, depending on a bedfrom size and shape, flow separation phenomena is observed at the dune leeside and influences significantly the energy dissipation between the overlying free water flow and the recirculating turbulent vortex shedding (Best, 2005; Cisneros et al., 2020; Lefebvre and Winter, 2016). Therefore, the the resistance coefficient of bedforms uncertainty becomes one of the main sources of errors in numerical modelling studies, and these errors increase dramatically while investigating extremely high water level conditions.

Earlier studies dealing with changes of bedform geometry performed in large sand-bed rivers during flood events showed that both, mean dune height and length increase as a function of the water discharge. Moreover, a hysteresis (loop-rating effect) can be observed for dune height and length, which indicates that, for a given water discharge, both dune size parameters are larger during the falling limb than for the period of the rising stage (e.g. Harbor, 1998; Julien and Klassen, 1995; Julien et al., 2002; Ten Brinke et al., 1999; Wilbers and Ten Brinke, 2003). Lagged response of dunes presents significant implications for flow hydraulics: in fact, dunes extract fluid momentum by form drag and therefore dune size has a significant effect on the bed friction factor, and moreover, large losses by form drag reduce the skin friction available for sediment transport as well (Martin and Jerolmack, 2013). As noted in Warmink (2014), dune evolution during rising limb of a flood wave is quite well understood and can be successfully modelled, however, dune evolution during the falling limb remains poorly understood yet. Also, Reesink et al. (2018) underlined recently that the precise mechanisms of dunes adaption to changes in water flow and knowledge of the hydraulic variables that control dune modifications in size and shape over time and space remain still insufficiently studied. Therefore, understanding physical processes accompanying changes in bedform geometry, their migration and how one responses to a changing water flow are of particular significance for river system management aimed primarily to accurately estimate water levels during normal and extreme hydrological conditions.

The development of high-resolution measurement techniques led to the availability of bottom relief data with unprecedented accuracy and hence lots of progress have been accomplished in different aspects of subaqueous bedform studies performed in natural environments during last decades (e.g. Barnard et al., 2013; Best et al., 2010; Hu et al., 2018; Koop et al., 2020; Lyons and Pouliquen, 2004; Parsons et al., 2005; Sambrook Smith et al., 2013). These measuring techniques, however, are of limited use during the extreme events, when navigating the vessel through abnormal hydraulic conditions becomes dangerous for the crew and equipment.

In order to fill this gap, this study provides the first insight into bedform morphodynamics during the passage of flood wave on a river of the Baltic Sea basin. The paper presents results of investigations of subaqueous sand dunes geometry in the Vistula River mouth performed before, during, and after the flood event. An analysis of high-resolution bathymetric dataset that permits: to quantify the Vistula dunes dimensions (dune height and length, steepness) together with their angularity (mean stoss- and lee-side angles), to determine dune development, and to calculate bed roughness due to dunes under more energetic hydrological conditions is presented here. A parametrization of relation between flow depth and dune height and an estimation of the potential for flow separation are performed as well. In addition, the spectral analysis of the bed elevation profiles allowed distinguishing regions in the riverbed morphology of the Vistula mouth, and highlighted a distinct behaviour of the power-law spectral functions. The outcome of the study could be pivotal for improving our understanding of bedload transport processes, could help in palaeohydraulic reconstruction studies in the area, as well as could be essential for calibration of numerical models of alluvial sand-bed large rivers, aiming to predict dune dynamics, bed resistance, turbulent flow and flood water levels.

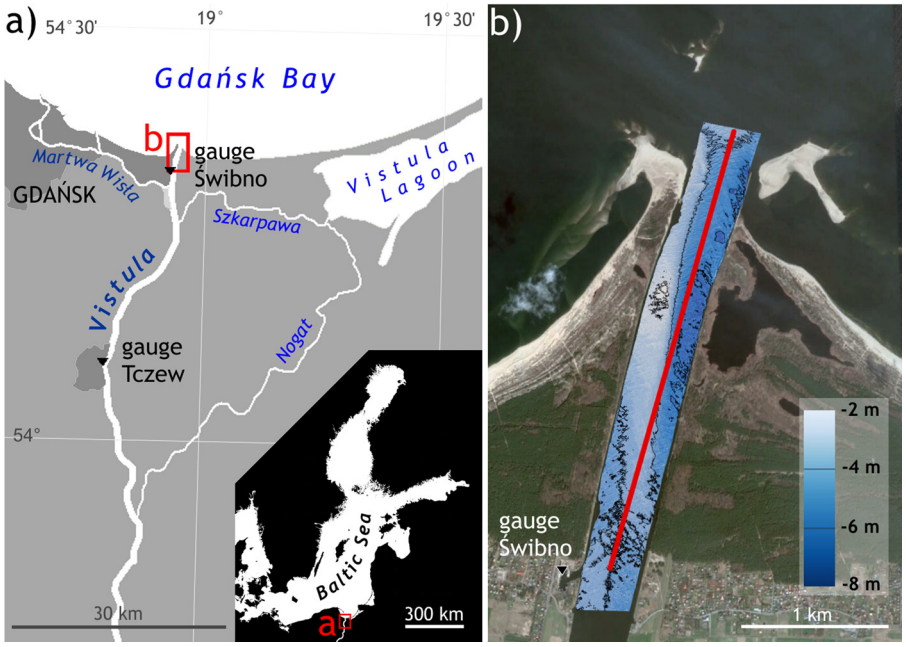

Figure 1 a) Location of the study area 'Przekop Wisły' in the southern Baltic Sea; b) Bathymetry of the Przekop Wisły surveyed in March 2014 (contours every 2 m) overlying an aerial photograph of April 2, 2014, together with the red centreline of 3270 m length along which the repetitive surveys were accomplished.

2. Material and methods

2.1. Geographical setting

The measurements were carried out in the main mouth of the Vistula River (Przekop Wisły) located in southern part of non-tidal Baltic Sea (Figure 1). The Vistula (Wisła) with the total length of 1047 km and the river basin of about 194 400 km^2 is the largest river in the region. The Vistula plays a dominant role both regards to the quantity of discharged fresh water flowing into the Gdańsk Bay and the sediment delivery. The river supplies about 7% of entire fresh water to the Baltic Sea with the average multiyear outflow amounting to 33.3 km^3 (Majewski, 2013).

The Przekop Wisły is a cross-cut artificial channel which was opened in 1895 (Szymański, 1897a,b) in order to protect Gdańsk city and nearby lowlands from floods. The intermittent catastrophic floods occurring previously, were effectively terminated (Makowski, 1995).

The channel has a total length of ca. 7000 m (starting at the Martwa Wisła lock; Figure 1a), ca. 400 m width and up to 8–9 m water depth. In the final 3000 m of the channel, a submerged sandbar crossing the channel diagonally from N to S is the most distinctive morphological feature (Fig. 1b). The riverbed is covered by complex patterns of rhythmic bedforms that were investigated recently by Lisimenka and Kubicki (2017). Results of granulometric analysis of grab samples revealed that the bottom sediments are characterized here by coarse and medium-grained sands (Rudowski et al., 2017).

Due to existing locks, about 95% of total Vistula water outflows into the Baltic Sea through this channel. Based on operational data obtained from the closest gauging station located in Tczew (31.2 km upstream, Figure 1a), which represents 99.9% of the total Vistula River catchment area (Majewski, 2018), the long-term (1921–2020) average annual water discharge reaches Q_{mean}=1020 m^3/s (IMGW-PIB, 2020). In the time span 1921–2020, the average daily water discharge ranged between a minimum of 238 m^3/s and a maximum of 9530 m^3/s (recorded during the flood event in April 1924, see Figure 2). In addition, based on the multiyear hydrological observations in Tczew, the Lower Vistula has an average ratio of maximum to minimum water discharge $<Q_{max}/Q_{min}>$=9.4, where Q_{max} and Q_{min} are the water discharges representative of the highest and lowest daily flows in a particular hydrological year, respectively. Records covering one century show that there have been 36 flood events with the water discharge higher than Q>4000 m^3/s. Amongst these, the flood event of May 2014 with the peak wave discharge Q_{peak}=4110 m^3/s belongs to the group of the highest high-water hydrological events (≈25th percentile of the century-long annual maximum flow values) that occurred in the area of interest.

2.2. Hydrological conditions during the experiment

The time series of the Vistula River discharge values, collected at the Tczew gauge in a period of experiment between 28.02. and 16.06.2014 (Figure 3a), revealed a passage of flood wave with the maximum intensity about four times higher than that of the long-term mean annual outflow. The peak wave with the discharge Q_{peak}=4110 m^3/s was observed in 25th of May 2014 (Figure 3b). Duration time of the observed flood wave was about 25 days (if Q_{mean} exceedance is considered), but in fact the water level stabilised after 10 days at Q=1500 m^3/s (Figure 3) and the peak discharge occurred for a short period of

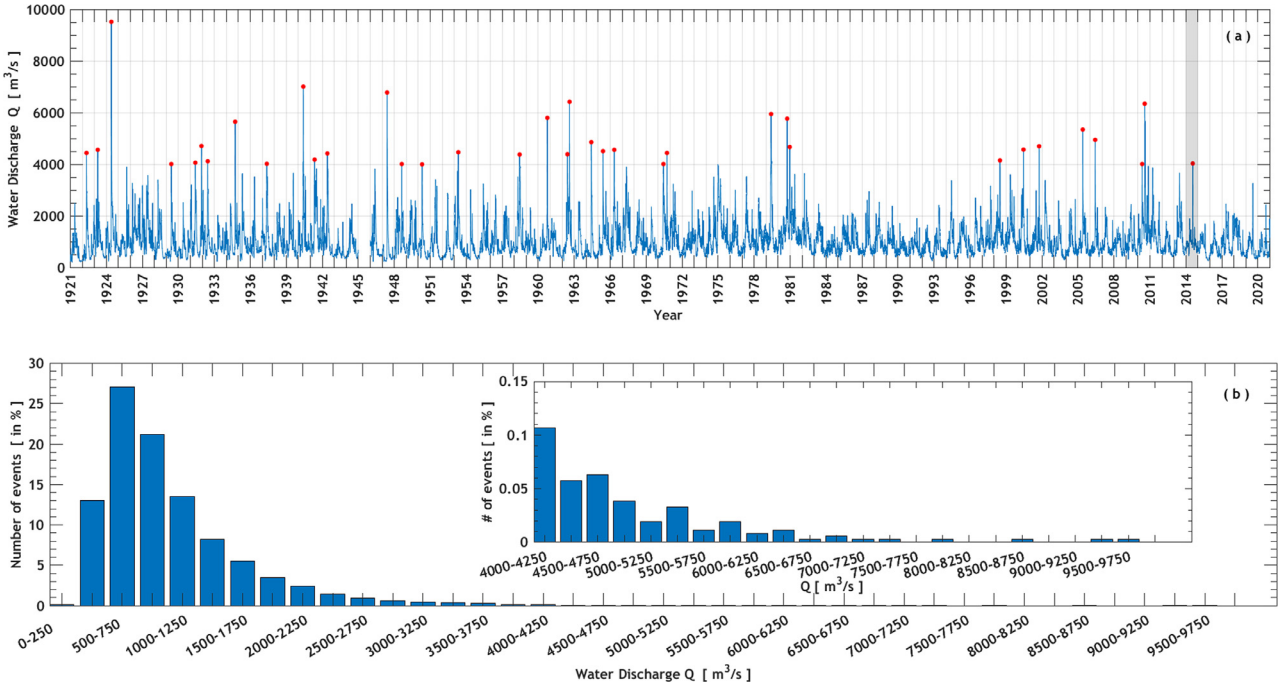

Figure 2 a) A century-long time series of the daily water discharges of the Vistula River at the Tczew gauge (see Figure 1a for location). Red dots mark flood events with the water discharge higher than Q>4000 m^3/s; b) Variations in discharges in 250 m^3/s intervals with largest discharges rescaled (IMGW-PIB, 2020).

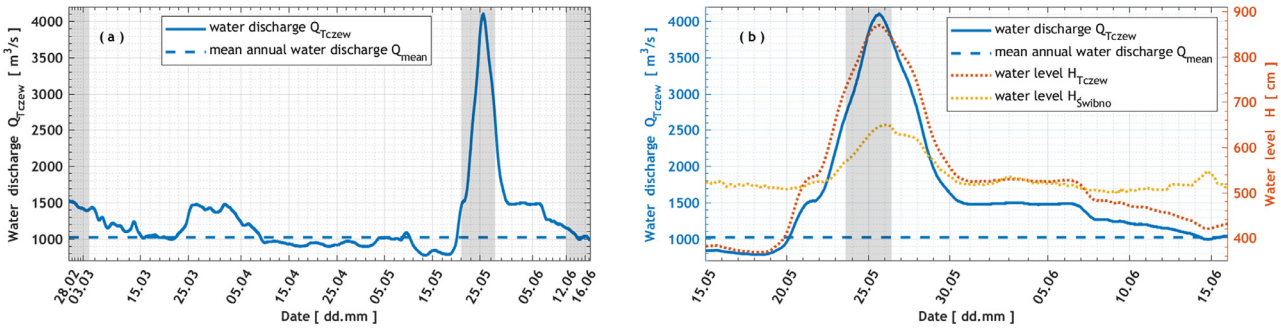

Figure 3 a) Discharge graph in the Lower Vistula between 28.02. and 16.06.2014. Time series of hourly water discharge Q_{Tczew} m^3/s (solid blue curve) in respect to long-term mean annual water discharge Q_{mean}=1020 m^3/s in Tczew (dashed blue line); b) time series of water discharge and water levels H cm at Tczew and Świbno gauges (see Figure 1 for location) in a period between 15.05. and 15.06.2014 (dotted dark and light brown curves, respectively). The grey rectangles indicate time periods of in-situ measurements (IMGW-PIB, 2020).

time, so the flood wave can be schematically classified as the sharp-peaked one. In accordance with Allen and Collinson's (1974) formulation $(\Delta Q/\Delta t)\cdot Q_{peak}^{-1}$ (where ΔQ is the change of discharge in a time step Δt), the characteristic rate of the rising limb between the long-term mean annual outflow Q_{mean} and the observed flood peak Q_{peak} was about of 0.125 per day. In turn, the characteristic rate of the falling stage was in the order of 0.04 per day. Essentially, such relatively fast changes in hydrological conditions are favourable to formation of superimposed bedforms, i.e., the smaller dunes overlaid on the larger ones (e.g., Allen and Collinson, 1974; Wilbers and Ten Brinke, 2003). Moreover, Paarlberg et al. (2008) observed that the shape of a flood wave influences dune dynamics in significant way. The authors underlined that the sharp-peaked flood wave characterized by the longer duration of the rising and falling stages gives subaqueous dunes less time to adapt to the higher (peak) discharge.

Based on cross-correlation analysis (using the Matlab® *xcov* function) performed on water level time series, the time lag of flood wave passage between Tczew and Świbno cross-sections (over distance of 31.2 km) was estimated at τ=8 h. Thus, an average speed of flood wave was evaluated at ca. 1.1 m/s what is in reliable agreement with the observed vessel drift speed (≈2 knots) during the measurements. The estimated flow speed is approximately twice faster (considering also the spatial variability of the flow field across the river channel) than the depth-averaged velocities observed during normal hydrological conditions (Lisimenka et al., 2015).

2.3. In-situ measurements

The measuring campaign was initially a part of regular half-yearly monitoring carried out in Vistula River mouth area within the project VISTULA No PBS1/A2/3/2012. Two months after the monitoring survey of March 2014 (28.02—03.03), heavy rains in the Upper Vistula basin initiated a flood wave. Additional surveys were organised in the Vistula mouth and undertaken between May 23 (flood beginning phase) and May 26, 2014 (flood peak phase) during the passage of the flood wave. The surveys initially planned until May 29 (flood end phase), were too dangerous to perform due to significant number of large debris floating on and just below the river surface. Therefore, the survey accomplished in June, 2014 (12.06—16.06) is treated here as flood end situation.

The boat-mounted Reson SeaBat 7101 multibeam echosounder (MBES) with the nominal working frequency of 240 kHz and ping rate up to 40 pings/s was used in all bathymetric surveys. The high-resolution multibeam sonar system provides up to 511 discrete across-track sounding beams and illuminates 150° swath on the seafloor (with 1.5° along-track transmit beamwidth, 1.8° across-track receive beamwidth and depth resolution 0.0125 m). The fixed-mount sound velocity probe Reson SVP-70 was installed on the MBES head aiming to permanent monitoring of the sound speed at the depth of the sonar head. The portable sound velocity profiler Reson SVP-15 was used to obtain the sound speed profile through the whole water column. The Trimble SPS 851 GPS Receiver with RTK-positioning (ensuring centimeter-level accuracy) together with the Ixsea Hydrins inertial navigation system (with r-p-h accuracy of 0.01°) were integrated with the MBES and SVPs using the QINSy data acquisition software package. In that way, the overall measuring error is estimated within 5 cm xyz. The initial post-processing of the MBES raw data were performed in the QINSy Processing Manager according to the IHO standard procedures used in hydrography.

2.4. Dune geometry determination and spectral approach

Determination of crest and trough positions of individual primary bedforms (Figure 4, red and green markers respectively) for all one-dimensional bed elevation profiles (BEPs) were performed based on the approach proposed by Van der Mark and Blom (2007). For each single bedform, dune height H defined as the vertical distance between a crest and its downstream trough and dune length λ defined as the horizontal distance between two subsequent crests were obtained. Additionally, the relationship between dune height and flow depth H/Z, dune steepness defined as H/λ ratio and the mean stoss- and lee-side angles were determined using simple geometric relations (see dune schematic concept presented in Cisneros et al., 2020).

The spectral analysis of the BEPs to obtain power spectrum density (PSD) estimates was performed by using the Matlab® *periodogram* function. After subtracting the mean depth and applying the detrending procedure by fitting and removing a five-order polynomial regression model, the variance spectra were determined for each flow rates. The smoothing of the obtained spectra was fulfilled with use of the DPSS taper function, i.e., discrete prolate spheroidal sequences or Slepian sequences, which are known as unique window functions which offer the best side-lobe suppression (Percival and Walden, 1993).

In context of the determination of the dominant dune lengths (local peaks of the spectra), the characteristic wavenumbers k_{ch} (and consequently λ_{ch}) were evaluated for all measurements based on the concept introduced firstly by Young (1995) in sea surface dynamics study. For this purpose, the author proposed to calculate the weighted integral of power 4 of the spectral function. This approach was applied also by Davis et al. (2004) as well as by Lisimenka and Kubicki (2017) in bedform studies:

$$k_{ch} = \frac{\int k \cdot S^4(k)dk}{\int S^4(k)dk} \text{ and } \lambda_{ch} = \frac{2\pi}{k_{ch}} \quad (1)$$

3. Results

The analysis of bed elevation profiles revealed a presence of asymmetrical small (with typical spacing λ=0.6—5 m), medium (λ=5—10 m) and large (λ=10—100 m) sand dunes according to the bedform classification scheme introduced in Ashley (1990).

Comparison of the successive bed elevation profiles indicated significant changes with time in conjunction with changing hydrological conditions. To start with, the number of dunes increased from N_1=478 up to N_2=630 in time period between the initial time step (Figure 4a) and the first survey during passage of the flood wave (Figure 4b). After that the number of individual dunes reduced considerably up to N_5=160 at the final stage of the rising limb (Figure 4e), so that to reduce even more up to N_6=134 at the next time step, i.e., at the beginning of the falling limb (Figure 4f), what is probably an effect of an amalgamation (merging) of the investigated bedforms. In turn, approximately the same number of dunes N_7=138 was identified in the last time step, i.e., two and half weeks later, when the hydrological regime of the river returned closely to the long-term average conditions.

The relationship between dune height H and flow depth Z for each time steps (Figure 5) shows that the vast majority (about 95%) of dunes observed in low hydrological conditions Q<1500 m^3/s (time steps Q_1 and Q_7, standard flows) fall below H=0.127Z approximation (Figure 5, dotted line). Moreover, for relatively low/moderate hydrology with Q<2500 m^3/s (including of time step Q_2 corresponding to the beginning of the rising limb) there are almost no dunes with height above H=0.17Z (Figure 5, dashed line), i.e., of about 96% of bedforms are below this line at all. In turn, about 75% of dunes observed in hydrological conditions higher than Q>2500 m^3/s (starting with time step Q_3; rising limb) fall above H=0.17Z. Interestingly, for the highest hydrological conditions observed in the experiment close to $Q\approx$4000 m^3/s, i.e., time steps Q_4 (rising limb), Q_5 (peak discharge) and Q_6 (beginning of the falling limb), a relationship between dune height and flow depth of H=0.33Z (Figure 5, dash-dotted line, see Wignall and Best, 2000; c.f. Cisneros et al., 2020) could be assumed as an 'upper boundary condition' for approximately 50% of dunes. It should be noted also that only 6 dunes (see grey patches in Figure 4f

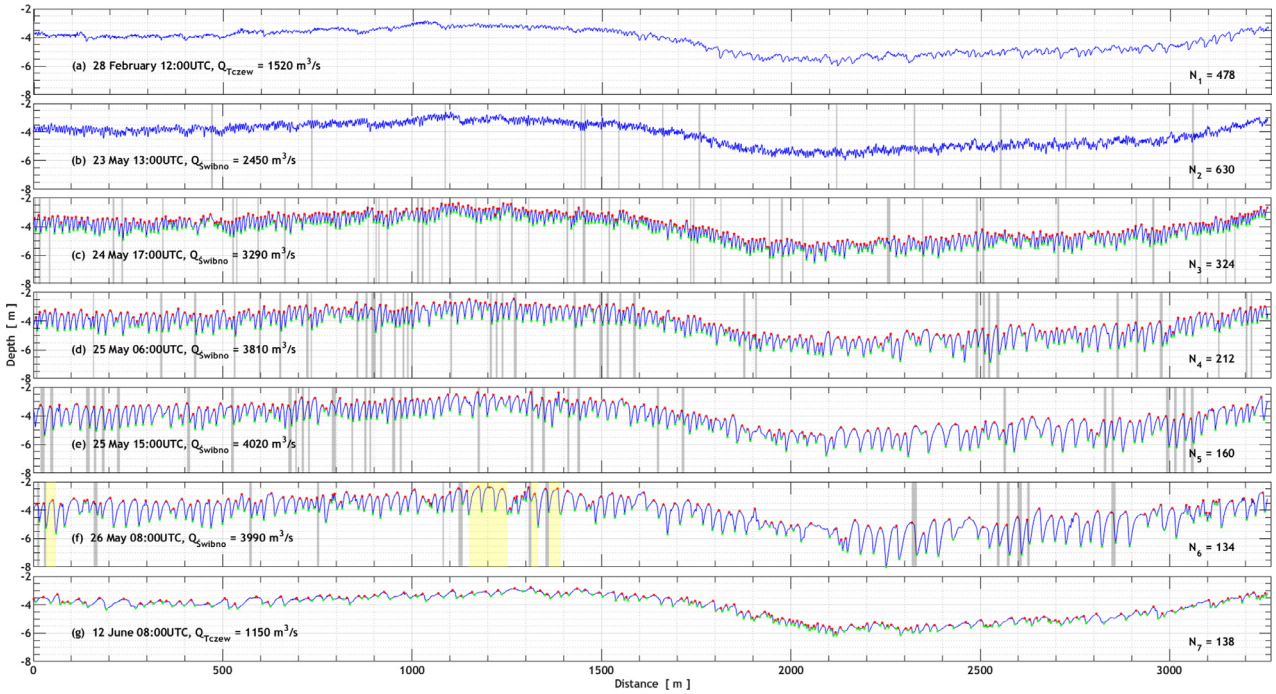

Figure 4 Bed elevation profiles (BEPs) along the centreline of 3270 m length with the appropriate date, time, water discharge value Q m^3/s and number of dunes N for all successive echosoundings. Location of crests and troughs depicted with red and green markers respectively (not shown for two first surveys due to readability). Grey patches mark lee-side slopes of the particular dunes with the potential for flow separation (based on findings of Lefebvre and Winter, 2016). Yellow patches mark six dunes with $H/Z>0.66$ (see Figure 5). *Note*: water discharges values $Q_{\acute{s}wibno}$ were calculated based on the obtained time lag (see Sec. 2.2).

for location) amongst the total number of 2076 examined in the whole experiment fall above $H=0.66Z$ (Figure 5, solid line).

For clarity, further in the text, the same concept of colours representing all hydrological conditions is applied in the following figures: Q_1=1520 m^3/s (blue), Q_2=2450 m^3/s (green), Q_3=3290 m^3/s (magenta), Q_4=3810 m^3/s (black), Q_5=4020 m^3/s (red), Q_6=3990 m^3/s (yellow) and Q_7=1150 m^3/s (cyan).

The scatter plot of dune heights vs. lengths (Figure 6a) reveals that, the greater number of dunes falls between the global average (grey line) and upper limit trends (black line) obtained by Flemming (1988). There is, however, an exception related to the initial and the final steps (corresponding to the lowest hydrological conditions observed in the experiment), at which the vast majority of dunes fall below the global mean trend, what could suggest that these bedforms are lower at these stages (Figure 6a, blue and cyan dots, respectively).

Naturally, in the context of the dune geometry a considerable reshaping was observed with time as well (Table 1). Analysis of the mean dune height and length vs. water discharge revealed a counter-clockwise hysteresis (Figure 6b, blue and brown curves respectively). For example, after the almost 3 months period of time between the initial time step and the first survey during the flood, a significant increase in the mean value of the dune steepness H_{mean}/λ_{mean} of about 3 times was observed (Figure 6c, blue curve), where the mean dune height increased from H_1=0.16 m and its standard deviation σ_{H1}=0.12 m up to H_2=0.35 m (σ_{H2}=0.16 m) while the mean dune length reduced from λ_1=6.8 m ($\sigma_{\lambda1}$=4.7 m) up to λ_2=5.2 m ($\sigma_{\lambda2}$=1.4 m). After that, during the first 28 h of the flood observation, in the course of which the water discharge increased gradually on ΔQ=840 m^3/s from Q_2=2450 m^3/s to Q_3=3290 m^3/s (almost the same increase of Q value as in preceding time period), the mean dune height and length both have risen to H_3=0.71 m (σ_{H3}=0.26 m) and to λ_3=10.0 m ($\sigma_{\lambda3}$=2.6 m), respectively. Successively, the mean dune height and length increased up to H_5=1.17 m (σ_{H5}=0.42 m) and λ_5=20.1 m ($\sigma_{\lambda5}$=6.4 m) at the final stage of the rising limb with Q_5=4020 m^3/s. In turn, at the beginning of the falling limb, the geometrical dimensions of the dunes increased even more up to H_6=1.28 m (σ_{H6}=0.6 m) and λ_6=24.1 m ($\sigma_{\lambda6}$=10.1 m). Finally, after 17 days during which the hydrological conditions in the Lower Vistula returned closely to the long-term average Q_{mean} (Figure 3), a significant reducing in dune steepness was detected – the mean dune height reduced of about 4 times while the mean dune length kept almost the same (comparably stable) by comparison to the time step corresponding to the beginning of the falling limb. Thereby, the highest dynamics in dune field changes was observed at the final stage of the rising limb during which the bedforms revealed growth with average rates about of 0.02 m/h in height and about of 0.5 m/h in length respectively, while the water discharge increased from Q_4=3810 m^3/s to Q_5=4020 m^3/s during about 9 hours only. However, the latter one could be attributed to a lack of

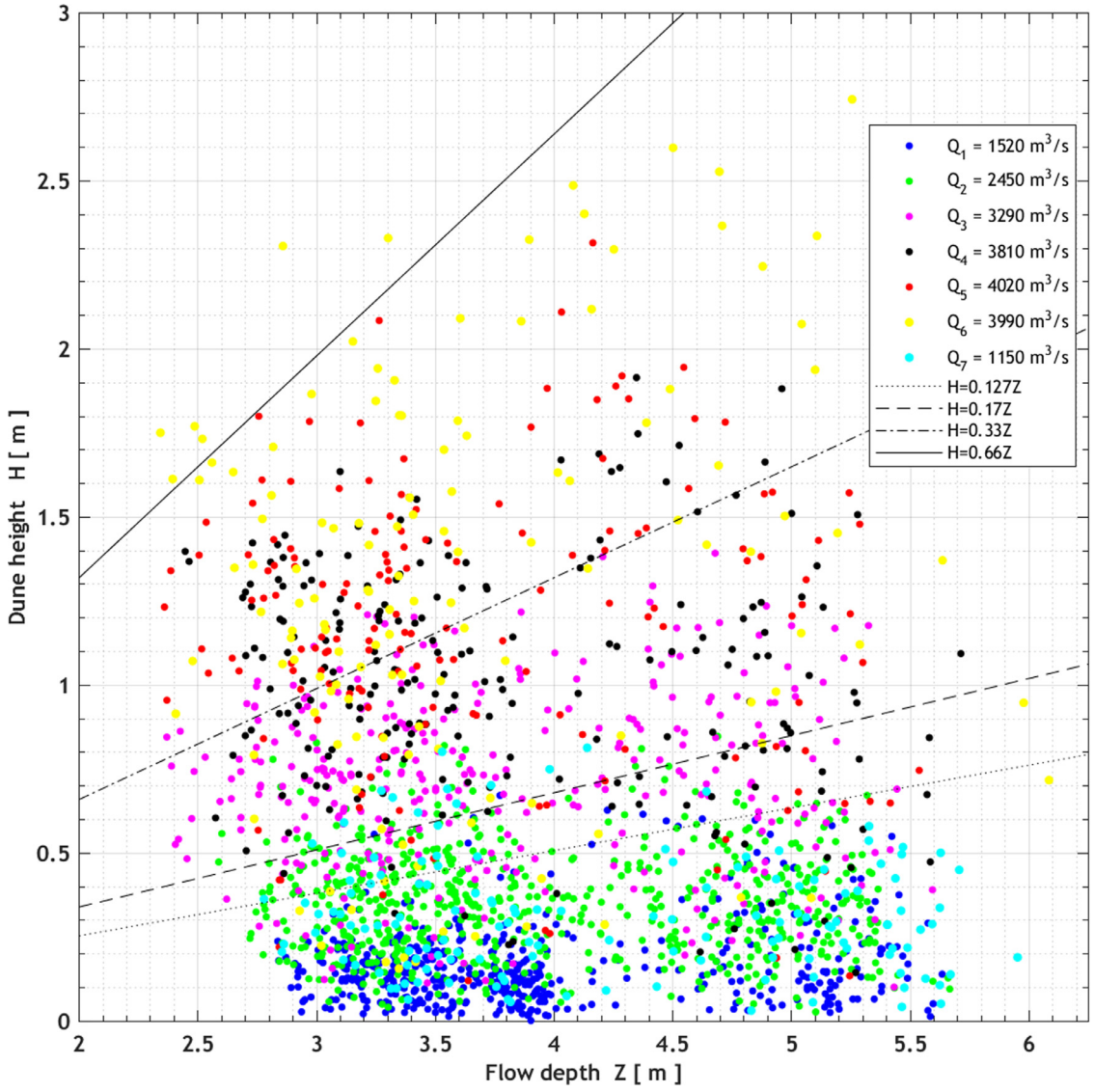

Figure 5 Plot of dune height H m versus flow depth Z m for all dunes observed in the experiment under changing hydrological conditions. The H/Z relationships for values equal to 0.127 (dotted line), 0.17 (dashed), 0.33 (dash-dotted) and 0.66 (solid), respectively.

a sufficient number of observations during the falling limb phase.

Besides, the bed roughness k_{dunes} related to dunes was calculated based on the empirical relationship obtained by Van Rijn (1984):

$$k_{dunes} = 1.1\gamma_d H_{mean}\left(1 - e^{(-25H_{mean}/\lambda_{mean})}\right) \quad (2)$$

where H_{mean} and λ_{mean} — the mean dune height and length respectively, and γ_d is the shape factor expressing the influence of the dune form on the roughness height, taking into account that according to Van Rijn (1993), γ_d equals to 0.7 for dunes observed in field conditions.

As shown in Figure 6c (brown curve), the bed roughness noticeably increases with water discharge with the lag-effect, like in the case of the dune height (anti-clockwise hysteresis). It should be also noted that for moderate (Q>2000 m^3/s) to high hydrological conditions, the bed roughness due to dunes is found to be of about 50%—63% of the mean dune height value of the primary bedforms, wherein the k_{dunes}/H_{mean} ratio is higher during the rising limb of the flood wave. In contrast, one reveals values of about 22%—37% during low hydrology (Q<1500 m^3/s).

The smoothed variance spectra corresponding to the particular hydrological conditions Q_1—Q_7 together with the appropriate locations of the characteristic wavenumbers k_{ch} (depicted with the diamond markers in according with the applied colour scheme) are presented in Figure 7.

In general, three scaling regions could be distinguished in the riverbed morphology of the Vistula mouth: the first one — the low-frequency part of the spectrum with wavenumbers below k<0.015 rad/m what corresponds to macroscale bedforms with lengths larger than of about λ>≈420 m, i.e. comparable or larger than the river width W. Behaviour of all of the spectra in this low frequency range is characterized by flat spectra, what could be potentially interpreted as a lack of influence of any large scale anthro-

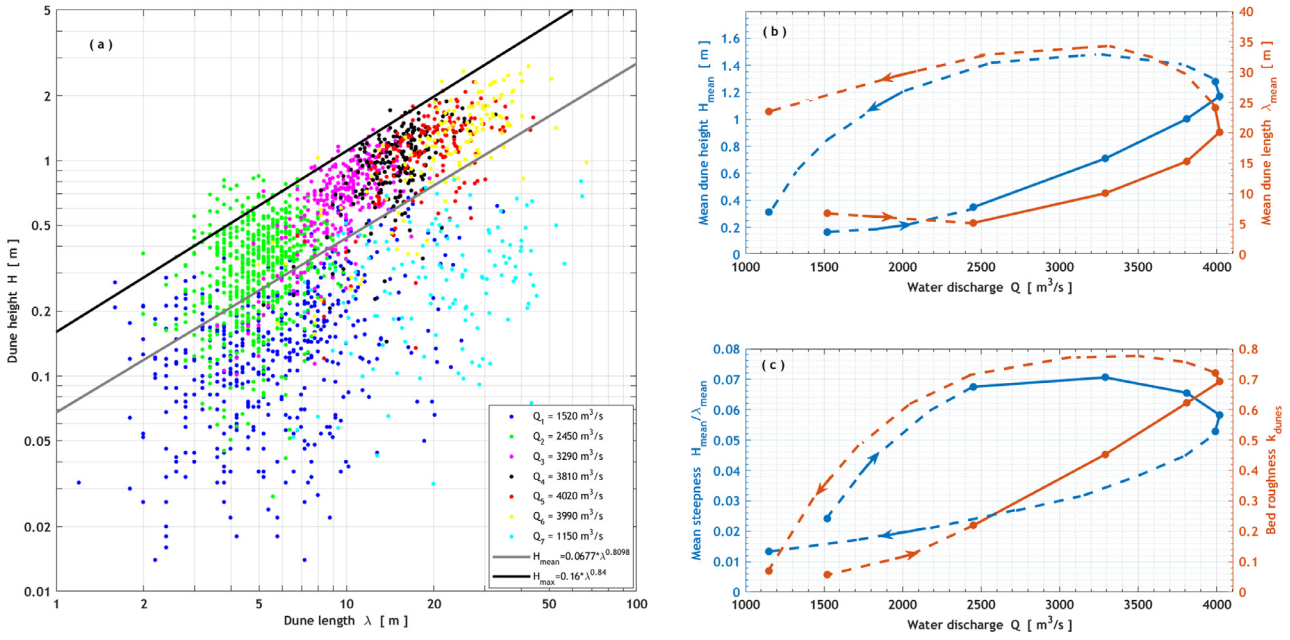

Figure 6 a) Plot of dune height H vs. dune length λ under changing hydrological conditions, overlapping the global average $H_{mean}=0.0677\lambda^{0.8098}$ (grey line) and upper limit $H_{max}=0.16\lambda^{0.84}$ (black line) relationships obtained by Flemming (1988). Development of dunes during flood: b) mean dune height H_{mean} m (blue curve; left y-axis) and dune length λ_{mean} m (brown curve; right y-axis); c) mean steepness H_{mean}/λ_{mean} (blue curve; left y-axis;) and bed roughness due to dunes k_{dunes} (brown curve; right y-axis).

pogenic factors (like river groynes or other hydrotechnical structures) on the riverbed morphology (at the investigated river stretch, the straight-segment riverbanks are strengthened by concrete and/or stony walls along the whole river channel). The second scaling region is the mesoscale one, which is characterized by a presence of a large sand dunes with lengths between of about $1\div2<\lambda<420$ m. In turn, the third region – the high-frequency 'tail' corresponds to microscale surface roughness with wavenumbers $k>2\pi$ rad/m, i.e. small dunes (with $\lambda<1$ m) and ripples.

The spectra show that with the development of the flood wave, the most significant changes of the riverbed morphology were observed in the 'mesoscale' frequency region between $0.094<k<\pi/2$ rad/m (i.e., for dune lengths between of about $2<\lambda<66$ m). Interestingly, in this 'transition region', the distinct behaviour of the spectra is observed. The 'low hydrology' spectra (blue and cyan curves in Figure 7) follow sufficiently well the power law function $S(k)\sim k^{\gamma}$, described by the spectrum slope $\gamma=-3$ (Figure 7, grey dashed line). However, during the moderate and high hydrological conditions (Q_2–Q_6 curves in Figure 7), the spectrum slope γ increases and all of the spectra follow by a '-4 power spectral law' (Figure 7, grey dotted line).

Analysis of the dune slope angles (the average slope of all grid samples from crest point to trough point or vice versa, for lee- or stoss-side angles respectively) revealed that greater number of dunes (83% of the total ones) are asymmetrical with the gentler stoss-side slope α in comparison to the steeper lee-side one β (Figure 8a). In turn, only of about 2% of the observed dunes are ideally symmetrical (triangular). With the development of the flood wave, the clockwise hysteresis of the mean stoss and lee angles vs. water discharge were found (Figure 8b, black and blue curves respectively). Moreover, significant increase of about 3 times in both of the mean angles was observed starting from the initial time step up to (in general) the final stage of the rising limb. During this period of time, the mean dune stoss- and lee-side slopes increased respectively from $\alpha_1=2.6°$ ($\sigma_{\alpha1}=1.1°$) and $\beta_1=3.6°$ ($\sigma_{\beta1}=1.8°$) up to values higher than about of $\alpha_{mean}\approx7°$ and $\beta_{mean}\approx10°$, with the maximum values of $\alpha_3=7.6°$ ($\sigma_{\alpha3}=2.0°$) and $\beta_3=10.6°$ ($\sigma_{\beta3}=3.3°$) observed at the time step corresponding to the pre-final stage of the rising limb with $Q_3=3290$ m^3/s. It should be noted that the dune slope angles returned to even slightly lower values at the last time step [$\alpha_7=1.7°$ ($\sigma_{\alpha7}=0.8°$) and $\beta_7=2.5°$ ($\sigma_{\beta7}=1.5°$)] in comparison with the initial time step during which nearly the same low hydrological conditions were observed.

4. Discussion

With the development of the flood wave, growth of dunes in height together with the diminishing number of individual dunes were identified in all subsequent time steps (Q_2 to Q_6), although with progressively reducing rates. The reduction can be explained by the different kinematics of the large-scale bedforms in comparison with the small-scale ones. It is well known that the reaction time needed to adapt to changes of flow conditions varies depending on bedforms geometric dimensions. Naturally, the small-scale bedforms are subjected to quick modifications, but the large-scale ones, inversely, may take longer period of time to change (e.g., Bridge, 2003; Guala et al., 2020; Venditti et al., 2016).

The presented dataset illustrates that dunes with small heights are dominant in the Vistula River mouth channel. For the overwhelming majority of dunes observed in low

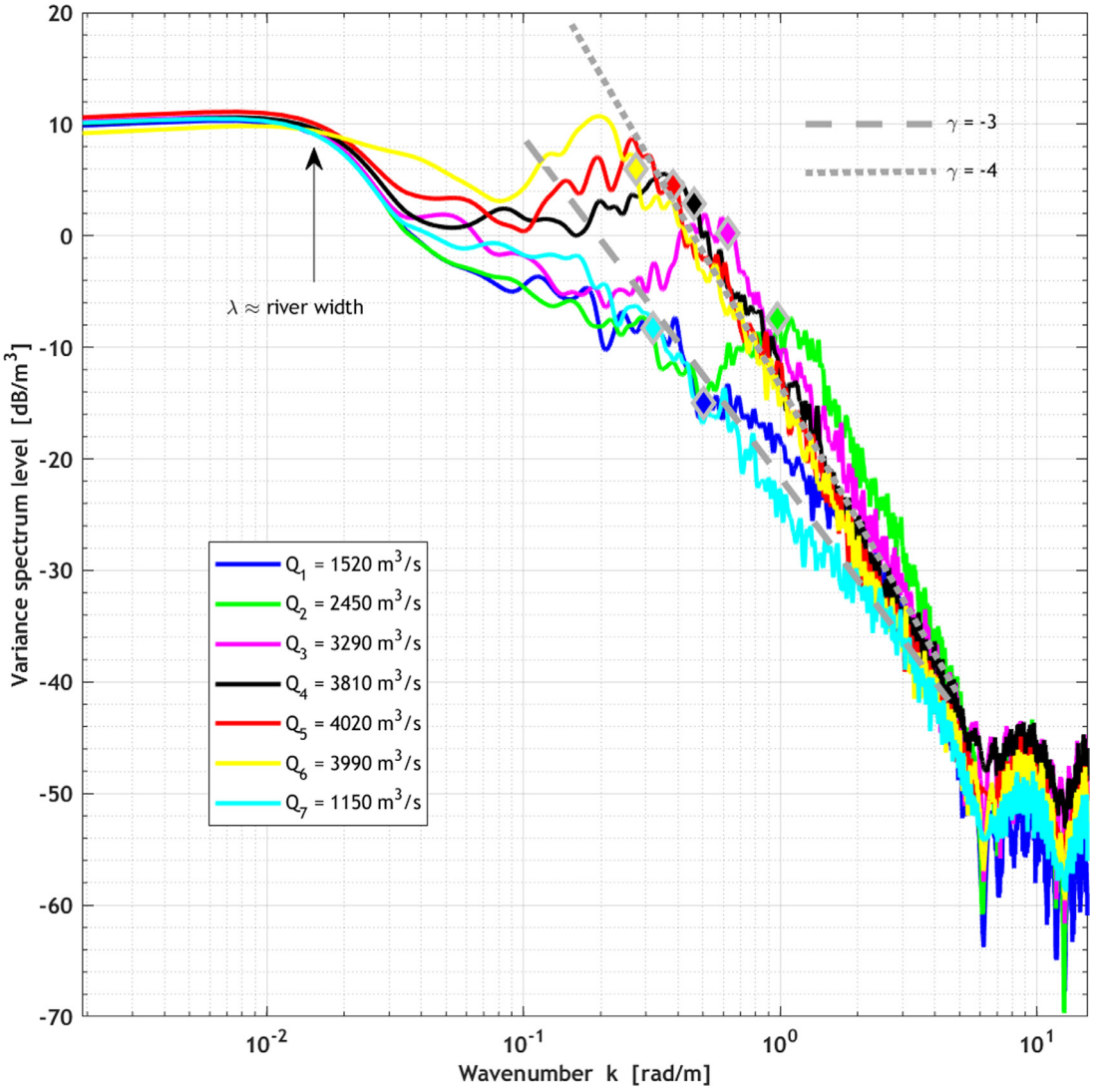

Figure 7 Variance spectra [dB/m^3] of the bed elevation profiles measured under changing hydrological conditions. Grey lines — power law functions with spectrum slopes γ=−3 (dashed) and γ=−4 (dotted), respectively. The black arrow appoints the scaling region corresponds approximately to the river width $\lambda \approx W$. The appropriate diamond markers determine the characteristic wavenumber k_{ch} obtained based on the Eq. (1).

hydrological conditions (Q<1500 m^3/s), the approximation H<0.127Z proposed recently by Cisneros et al. (2020) for deep flows (Z>2.5 m) could be representative for collected dataset. In turn, a value of H=0.17Z (Rubin and McCulloch, 1980) reflects well the maximum dune height that bedforms attain during moderate hydrology (up to Q≈2500 m^3/s). It is worth to note that the largest submerged dune heights with H>0.66Z (with a maximum value of 0.8Z) were observed at the beginning of the falling stage of the flood hydrology (Q≈4000 m^3/s) for six bedforms only located at shallower part of the river with depths about of Z=2.3−3.3 m. However, due to lack of sufficient data samples related to the falling limb phase of the examined flood, it is rather difficult to establish if there were any more individual dunes with heights higher than H=0.66Z, although some growth of dunes in height could potentially be observed at the next few time steps after the beginning of the falling limb (Figure 6b).

A noticeable anti-clockwise hysteresis (lag effect) was detected both between dune height H or length λ and water discharge (Figure 6b), where H and λ are substantially out of phase with progressive changes of Q. Such phenomena of the subaqueous dune evolution occurs only when the time scale of water discharge change is faster than the bedform adjustment time and specifically more pronounced lags are observed in the case of 'fast flood waves' (Martin and Jerolmack, 2013). In general, our observations are in agreement with the results of investigations performed by other authors in large sand bed rivers. The findings of earlier studies indicate that dunes are observed to grow during the rising limb, reach their maximum size after peak discharge and decay in size as the flood recedes (e.g., Amsler and Garcia, 1997; Julien and Klassen, 1995; Julien et al., 2002; Ten Brinke et al., 1999; Wilbers and Ten Brinke, 2003).

Even though there is a lack of data sets collected during the falling limb, different behaviour of the primary ge-

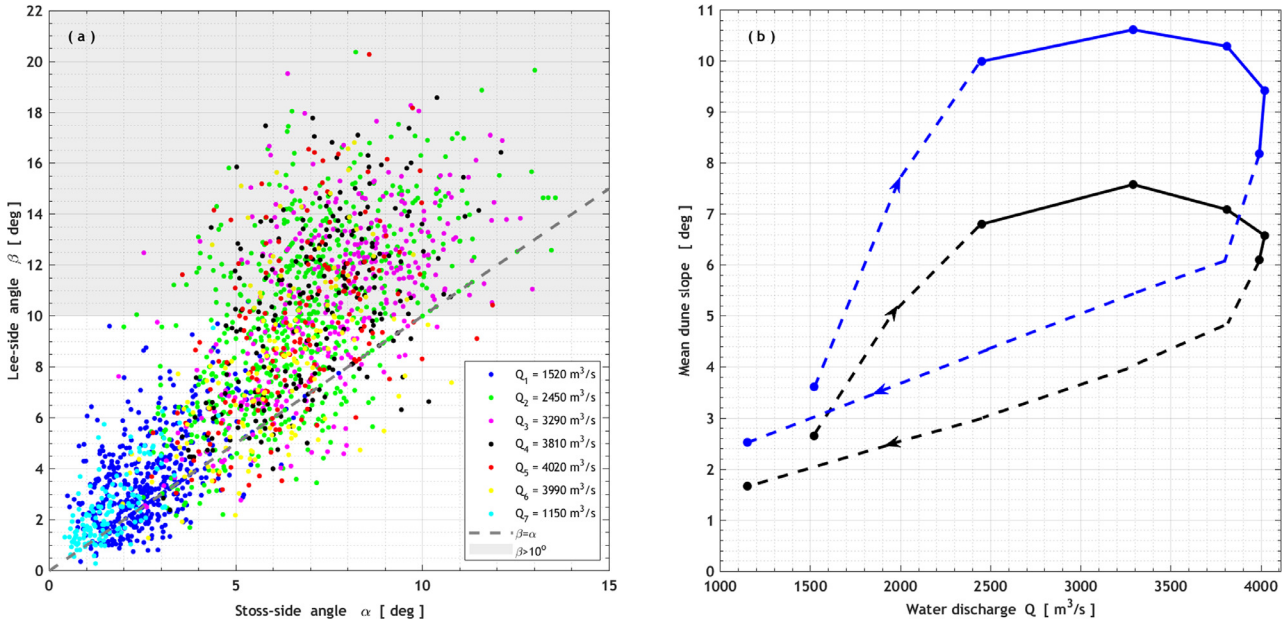

Figure 8 a) Plot of the lee-side angle β vs. stoss-side angle α (in degrees) under changing hydrological conditions. The dashed grey line marks dune symmetry condition $\beta=\alpha$. The grey patch indicates lee-side angles $\beta>10°$; b) Clockwise loops for the mean dune slopes of stoss-side angle (black curve) and lee-side angle (blue curve) as a function of the water discharge.

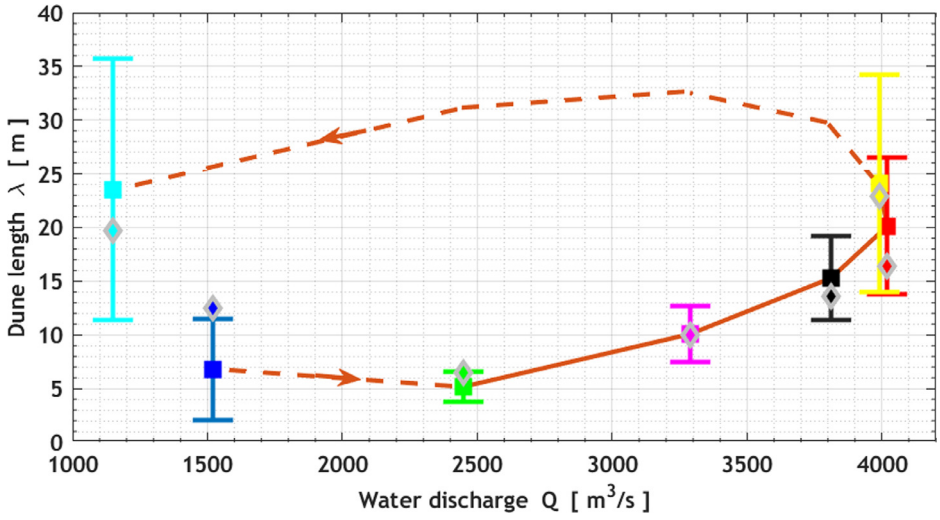

Figure 9 Development of dune length under changing hydrological conditions. Statistically derived mean dune lengths λ_{mean} m (square markers) with the whiskers indicating the standard deviation. Characteristic dune lengths λ_{ch} m (diamond markers) derived from spectral analysis on the basis of the Eq. (1).

ometry parameters (H and λ) of the Vistula dunes could be distinguished. The observed dunes show quick growth both in H as well as in λ when the water discharge increases, starting especially from the moderate hydrological conditions. In turn, when the hydrology starts to back close to the initial (long-term average) one, H decreases definitely with higher dynamics in comparison to λ. Although some indefinite growth of dunes size could be expected after the flood peak [e.g., dunes start to decrease only in size halfway through the flood falling limb according to Martin and Jerolmack (2013)], λ does not reveal a significant change at the final time step at all (in relation to the previous survey which corresponds to the initial stage of the falling limb). The probable explanation could be the erosion of dune crests and subsequent deposition of the material in the dunes troughs — in that way, low dunes in height, but long in length may form. In general, it is in agreement with the field observations performed by Wilbers and Ten Brinke (2003) of sand and sand-gravel bed reaches of the Dutch Rhine. Notwithstanding, the authors did not observe the dune length change in response to the varying water discharge in the sand bed section of the Waal River characterized by nearly the same granulometric composition of river bottom sediments consisted of medium to coarse-grained sands like in the Vistula River mouth (Rudowski et al., 2017). Likewise, results of laboratory observations and numerical

Table 1 Statistics of dune geometry during the passing flood.

# of time step	Water discharge Q [m³/s]*	# of dunes	Dune height H [m]			Dune length λ [m]				Dune steepness H/λ [-]			Bed roughness	Stoss-side angle α [deg]			Lee-side angle β [deg]		
			mean H_{mean}	median H_{50}	stand. dev. σ_H	mean λ_{mean}	median λ_{50}	stand. dev. σ_λ	characteristic λ_{ch}**	mean H/λ_{mean}	median H/λ_{50}	stand. dev. $\sigma_{H/\lambda}$	k_{dunes}	mean α_{mean}	median α_{50}	stand. dev. σ_α	mean β_{mean}	median β_{50}	stand. dev. σ_β
1	1520	478	0.16	0.14	0.12	6.8	5.6	4.7	12.5	0.029	0.025	0.021	0.06	2.6	2.5	1.1	3.6	3.3	1.8
2	2450	630	0.35	0.35	0.16	5.2	5.0	1.4	6.5	0.070	0.066	0.034	0.22	6.8	6.7	2.0	10.0	10.0	3.4
3	3290	324	0.71	0.72	0.26	10.0	10.0	2.6	10.0	0.070	0.072	0.021	0.45	7.6	7.7	2.0	10.6	11.0	3.3
4	3810	212	1.00	1.00	0.35	15.3	15.3	3.9	13.6	0.066	0.065	0.019	0.62	7.1	7.1	1.8	10.3	10.5	3.4
5	4020	160	1.17	1.20	0.42	20.1	19.3	6.4	16.4	0.060	0.060	0.019	0.69	6.6	6.6	1.8	9.4	9.1	3.5
6	3990	134	1.28	1.25	0.60	24.1	23.6	10.1	22.9	0.054	0.053	0.019	0.72	6.1	6.1	1.7	8.2	8.0	3.3
7	1150	138	0.32	0.29	0.17	23.6	21.2	12.2	19.7	0.016	0.012	0.011	0.07	1.7	1.5	0.8	2.5	2.2	1.5

* Water discharge values Q correspond to the time steps t_2–t_6 were calculated based on the obtained time lag τ=8 h (see Sec. 2.2).

** Characteristic dune length derived from spectral analysis of the BEPs on the basis of the Eq. (1).

simulations of bedform response to flow variability accomplished by Nelson et al. (2011) also revealed that when the flow decreases back to the original discharge, H quickly decreases in response, but λ decreases much more slowly. Using an unsteady two-dimensional flow model, the authors predicted much slower rate of λ increase during the rising limb and observed that one remains essentially constant, rather than decreasing, during the final low-flow period.

The result of our observations exposes a relatively greater growth in H *versus* λ reflecting in significant steepening of dunes (of about 3-fold) during a period of time between the origin phase and the flood peak approaching (dunes tend to steepen from 0.024 up to ≈0.07). Subsequently, around the flood peak, slight decreasing in the mean dune steepness was found (up to 0.06) with clearly visible further tendency of H/λ to reduce crucially (of about 4-fold) forward close to the origin stage. In that way, contrary to the dune height and length lag effects, the dune steepness reveals the clockwise hysteresis (Figure 6). It is worth noting that the observed variability of dune steepness is in general agreement within the ranges obtained in other field studies (Carling et al., 2000; Julien and Klassen, 1995; Julien et al., 2002). Furthermore, the relationship H/λ_{max}=0.16$\lambda^{-0.16}$ proposed by Flemming (1988) as the maximum limit trend effectively exemplifies a range of steepness for the dunes observed in the measurements (Figure 6a, black line). Besides, dunes with steepness lower than H/λ≈0.06 (Figure 6a, grey line) are either considered as a non-equilibrium bedforms (in our case, the ones observed at low hydrological conditions mainly) or, as noted in Carling et al. (2000), represent an equilibrium adjustment of the bedform, in which maximum steepness is precluded by hydraulic constraints, notably a depth limitation. On the other hand, real world observations suggest that equilibrium bedforms (the ones with consistent geometry/shape during their migration) are relatively rare in flood conditions and that subaqueous dunes evolve dramatically over the time scale of real floods (Nelson et al., 2011) what is confirmed thoroughly by our observations. In fact, tracking of the individual dunes was impossible to achieve as the latter ones were undergoing rapid changes under the varying hydrological conditions and, moreover, surveys were done rather too rarely in order to identify particular dunes on the subsequent records (*see* Figure 4).

By analysing the subsequent roughness spectra in context of localization of its local spectral peaks (Figure 7), the anticlockwise hysteresis effect both for H (spectrum level) and λ (wavenumber) may be inferred by the spectral method as well, confirming in that way the considerable reshaping of the dune field with time. It is visible that the dominant local peaks of the particular spectra change its x-y positions, repeating in this manner behaviour of the primary geometry parameters H and λ (Figure 6b). Naturally, it reflects re-organization of the dune field with time — sand dunes with the smaller heights and shorter lengths are swallowed by the bigger ones, creating the new bedforms which are become appropriately higher and longer than the two initial ones. In that way, high frequency spectral peaks are gradually shifted towards the low wavenumbers (i.e. increasing of λ) with the simultaneous growth of their spectral levels (i.e. increasing of H). Finally, spectral level of the dominant local peak of the 'end of the flood' spectrum (Figure 7, time step

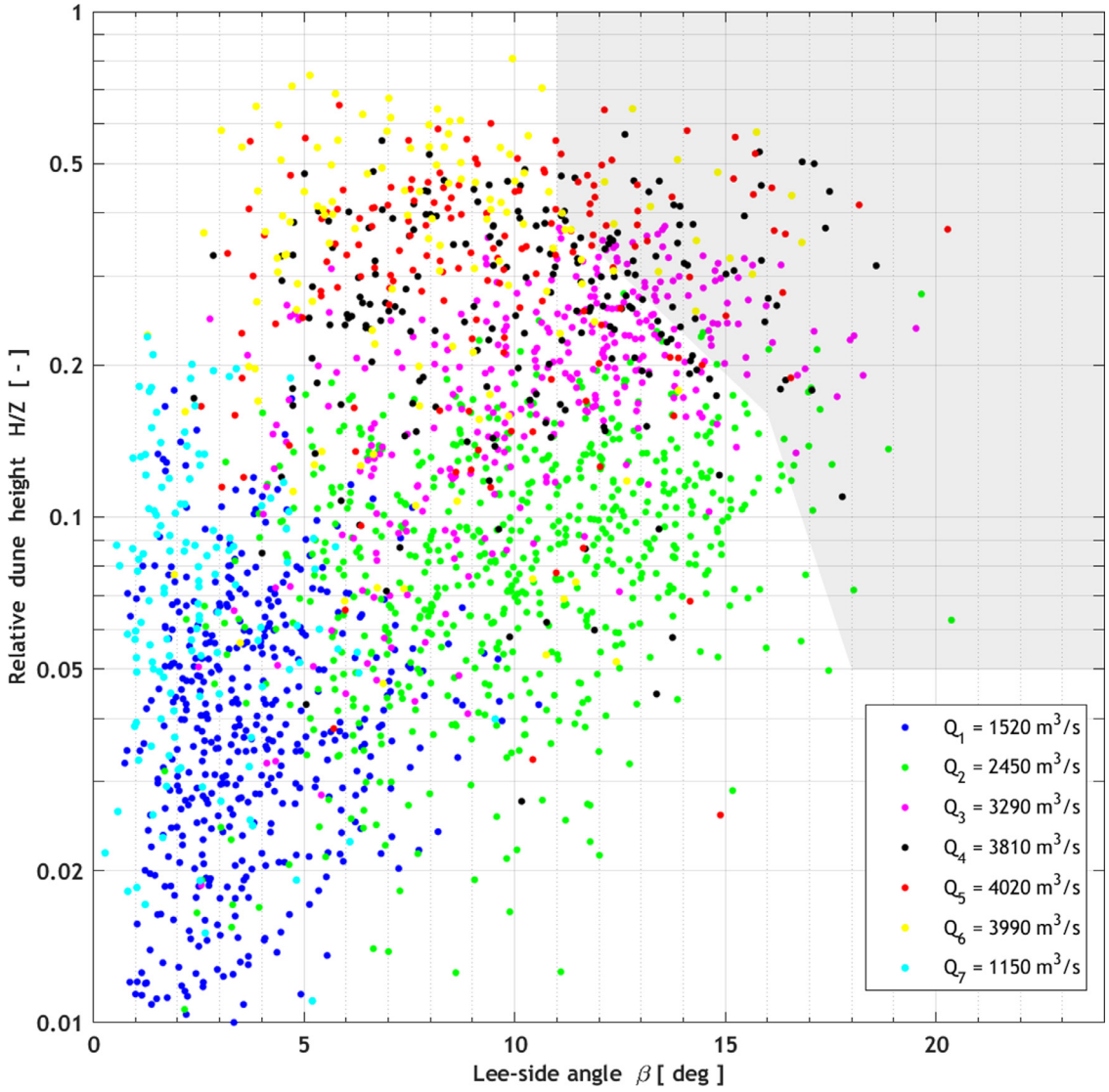

Figure 10 The potential for flow separation. Plot of lee-side angle β [deg] vs. relative dune height H/Z under changing hydrological conditions. The grey area indicates the minimum boundary conditions for β and H/Z at which, according to Lefebvre and Winter (2016), the onset of permanent flow separation could be observed.

Q_7) is abruptly dropped with keeping its almost the same position in the wavenumber domain, confirming reducing of the dune height, but keeping the dune length (i.e. reducing the dune steepness).

Furthermore, for low flow rates (average/standard hydrological conditions), the observed spectra could be approximated by the power-law fitting functions with the spectrum slopes close to $\gamma=-3$, especially at the mesoscale region, where the most significant dune field reshaping was observed (Figure 7, grey dotted line). This is in general agreement with the classic findings of Hino (1968), and confirms also the results of investigations performed by other authors (e.g., Aberle et al., 2010; Nikora et al., 1997). However, with the development of the flood wave, significant deviation from the '−3 power law' is observed — all of the spectra obtained at the moderate and high flows (Figure 7, time steps Q_2–Q_6) are characterized by the steeper spectrum slopes close to $\gamma=-4$ (Figure 7, grey dashed line).

Interestingly, comparison of behaviour of the (mean) dune lengths derived statistically λ_{mean} and the characteristic dune lengths λ_{ch} obtained based on spectral analysis under changing water discharge Q (Figure 9, square and diamond markers, respectively) revealed anti-clockwise hysteresis almost the same in both cases. Dune length values derived spectrally are, in general, in full agreement with the statistical values of λ, taking also into account the appropriate standard deviations σ_λ for the particular time steps. Nevertheless, it should be noted that at the time step corresponds to the initial phase, the spectrally derived λ_{ch} is out of whiskers, what could be explained by a presence of large numbers of relatively small-scaled dunes which significantly reduce the statistical mean at this particular time step.

In the context of the angular geometry of bedforms, our results exhibit the ubiquity of low-angle dunes, in vast majority with the asymmetrical shapes. Specifically, dunes

with the mean lee-side slopes milder than β=10° are fully dominant in low hydrological conditions (Figure 8a, time steps Q_1 and Q_7). According to the results of the numerical simulations performed by Lefebvre and Winter (2016), regardless of dune size and flow depth, a flow separation zone does not development over such low-angle dunes (lack of a zone of permanent flow separation). It could give an answer (at least partly) to the question raised by Warmink (2014) in relation to an existence of the flow separation behind such non-equilibrium bedforms with relatively large lengths (and small heights) observed at the final stage of the falling limb (see Figures 6a, 10). Moreover, in our case, about 70% of the 'low hydrology' dunes are characterized by the mean lee-side angles β<4° what could be evidence of an absence of a hydraulic effect at all (e.g. Cisneros et al., 2020). In the case of low-angle dunes, flow field structure characterizes by lower turbulence production dominated by eddies generated along shear layer, with a much smaller velocity differential than is characteristic of shear layers caused by flow separation in the lee side of classic angle-of-repose dunes. Consequently, lower energy losses between the recirculating flow and overlying free water flow are observed what results in weakening of flow resistance caused by (low-angle) dune form roughness (Best, 2005; Best and Kostaschuk, 2002).

With the development of flood wave, number of asymmetric dunes with lee-side angles β>10° significantly increases. Moreover, clockwise loops are observed both for stoss- as well as lee-side angles, with higher magnitude in the case of the last ones (Figure 8). It could suggest a probable appearance of recirculating flow (at least with intermittent origin) and its impact on steepening of lee-side slopes of particular dunes (Figure 4).

Findings of Lefebvre and Winter (2016) revealed that the minimum angle at which a flow separation zone is detected depends on the relative dune height H/Z. The authors determines the range of lee-side angles at which the flow separation is found to be present from β_{min}=11° for H/Z=0.4 to β_{min}=18° for H/Z=0.05 and predict an absence of the one for bedforms with a relative height H/Z=0.16 (Figure 10). In that way, total number of 146 dunes, which fulfil the mentioned above conditions were identified (points inside the grey polygon in Figure 10), what is of about 7% of the total number of dunes (2076 ones) examined in the experiment. It should be noted that with the development of the flood wave, the potential of flow separation increased gradually from 2.2% (at $Q_2\approx$2500 m^3/s), through 14.2% (at $Q_3\approx$3290 m^3/s), 18.4% (at $Q_4\approx$3810 m^3/s) up to 20% at the flood peak ($Q_5\approx$4020 m^3/s), in order to start to decrease to 11.1% at the beginning of the falling limb ($Q_6\approx$3990 m^3/s).

5. Conclusions

Subaqueous dunes in the mouth of the Vistula River to the non-tidal Baltic Sea share their geometric characteristics with bedforms of other large sand-bed rivers and fluvial environments. For the Vistula dunes, composed mainly by coarse and medium-grained sands, the global trend described by the exponential relationship between their height and length $H_{mean}=0.0677\lambda^{0.8098}$ proposed by Flemming (1988) and interpreted as an equilibrium condition could be a limiting factor indicating rather lack of sufficient sediment supply from the upper parts of the river, i.e., dunes are definitely underdeveloped at low hydrological conditions. Naturally, with increasing of water flow strength, ones indicate a tendency to grow both in height as well as in length and, in turn, are in a good agreement with Flemming's upper limit trend relationship $H_{max}=0.16\lambda^{0.84}$.

The present dataset reveals also that dunes with relatively small heights are absolutely dominant in the Vistula River mouth and the vast majority of rhythmic bedforms (about 95%) observed at low (Q<1500 m^3/s) to moderate hydrological conditions (Q<2500 m^3/s) could be characterized by the relationship between dune height against flow depth in range of $H/Z\approx$1/8÷1/6, respectively. In turn, the relationships H/Z=1/3÷2/3 could be assumed as upper limits for approximately 50% of dunes observed at high hydrology (Q>3800 m^3/s).

In context of the dune geometry, significant reshaping of the Vistula dune field was observed with the development of the examined flood wave. The mean dune height and length vs. water discharge revealed the anti-clockwise hysteresis (the lag effect). Based on our observations, starting from low hydrological conditions and up to the time step corresponding to the flood peak, the mean dune height and length increased successively from H=0.16 m and λ=6.8 m to H=1.17 m and λ=20.1 m, in order to increase even more up to H=1.28 m and λ=24.1 m at the beginning of the falling limb. Moreover, different behaviour of the primary geometry parameters (H and λ) of the Vistula dunes could be distinguished during the rising and falling limbs. The dune height decreases definitely with higher dynamics in comparison to the dune length during the falling phase, indicating in that way a significant decrease in dune steepness. During a period of time when the river returns to the long-term average hydrological conditions after the passage of the flood peak wave, the mean dune height was reduced about 4-fold while the mean dune length was almost the same by comparison with the time step corresponding to the beginning of the falling limb.

The spectral analysis of the bed elevation profiles led to distinguishing three scaling regions that corresponded to micro-, meso- and macroscales. Specific patterns of the spectra are observed in dependence on hydrological conditions. At the mesoscale region, where the most significant dune field changes were observed, the exponent of the spectral function $S(k)\sim k^{\gamma}$ is to be found close to '−3 power law' for low hydrological conditions, which is in agreement with the 'classic' assumption obtained firstly by Hino (1968). However, during the moderate and extreme hydrological conditions, spectra are characterized definitely by the steeper spectrum slopes close to or slightly higher than γ=−4. Furthermore, determination of the characteristic dune length λ_{ch} derived 'spectrally' could be a good alternative to 'the statistical approach' aiming to get an information about dominant dune length in bed elevation profile by finding the local peak position in the wavenumber domain of the spectrum. It was shown that the characteristic (dominant) dune lengths derived 'spectrally' are in general agreement with the ones derived 'statistically' (taking into account the standard deviation), showing the same pattern of the lag-effect as well. It could confirm the usefulness of the spectral approach in dune field analysis.

Analysis of the angular geometry of the Vistula dunes revealed supremacy of low-angle bedforms, in vast majority with the asymmetrical shapes. In general, of about 83% of dunes are characterized by gentler stoss-side slope α in comparison to the steeper lee-side one β, with only of 2% of the total number of ones which are ideally triangular. Definitely, dunes with the mean lee-side slopes milder than β=10° are fully dominant in low hydrological conditions. What is more, of about 70% of the 'low hydrology' dunes are characterized by the mean lee-side angles β<4° what, in turn, could be a reason for weakening of flow resistance caused by dune form roughness due to a complete absence of a hydraulic effect. With the development of flood wave, clockwise loops were observed both for the mean stoss- as well as lee-side angles, with higher magnitude in the case of the last ones. This could suggest a probable appearance of recirculating flow (at least with intermittent origin) and its impact on steepening of lee-side slopes of particular dunes (see Figure 4). Interestingly, it was observed that stoss- and lee-side angles behaviour as a function of the water discharge is the same as dune steepness taking into account clockwise hysteresis, with almost identical step-by-step analogy in evolution in the case of the stoss-side angles. In addition, based on findings of Lefebvre and Winter (2016) regarding criteria of probable appearance of flow separation, a relatively low number of dunes — of about 7% only (amongst 2076 of the total ones examined in the experiment) were identified as a fulfilling the mentioned above conditions (i.e., the appropriate range of lee-side angles β and relative heights H/Z). Notwithstanding, with the increasing of flow strength, it was observed that the potential of flow separation was increased of about 9-fold, from 2.2% at the flood beginning phase up to 20% at the flood peak and dropped abruptly up to 11.1% immediately at the beginning of the falling limb. Importantly, dunes with lee-side angles β>24° (with a fully developed flow separation zone) were not observed at the experiment at all, independently on hydrological conditions.

The data presented in the study could be an essential basis for creation of fluid dynamics models of natural bedforms in large sand-bed river channels, aiming to predict accurately dune dimensions and their evolution, flow resistance caused by bedform roughness, turbulent flow, as well as water levels during extreme hydrological conditions, for proper river system management.

Acknowledgements

The authors are grateful to the National Centre for Research and Development (Poland) for funding this work by grant VISTULA No PBS1/A2/3/2012. We wish to thank to our colleagues from the Department of Operational Oceanography of the Maritime Institute for their help in preparing and carrying out the bathymetric survey. Comments of two anonymous reviewers greatly enriched the manuscript.

Declaration of competing interest

The authors declare that there is no conflict of interest with third parties and that they have no known competing financial interests or personal relationships that could have appeared to influence the work reported in this paper.

References

Aberle, J., Nikora, V., Henning, M., Ettmer, B., Hentschel, B., 2010. Statistical characterization of bed roughness due to bed forms: A field study in the Elbe River at Aken, Germany. Water Resour. Res. 46, W03521. https://doi.org/10.1029/2008WR007406

Allen, J.R.L., Collinson, J.D., 1974. The superimposition and classification of dunes formed by unidirectional aqueous flows. Sediment. Geol. 12, 169—178.

Amsler, M.L., Garcia, M.H., 1997. Sand-dune geometry of large rivers during floods. J. Hydraul. Eng. 123, 582—585.

Ashley, G.M., 1990. Classification of large-scale subaqueous bedforms: a new look at an old problem. J. Sediment. Res. 60, 160—172. https://doi.org/10.2110/jsr.60.160

Barnard, P.L., Erikson, L.H., Edwin, P.L., Elias, E.P.L., Dartnell, P., 2013. Sediment transport patterns in the San Francisco Bay Coastal System from cross-validation of bedform asymmetry and modeled residual flux. Mar. Geol. 345, 72—95. https://doi.org/10.1016/j.margeo.2012.10.011

Best, J.L., 2005. The fluid dynamics of river dunes: a review and some future research directions. J. Geophys. Res. Earth Surf. 110, JF000218.

Best, J.L., Kostaschuk, R., 2002. An experimental study of turbulent flow over a low-angle dune. J. Geophys. Res. Oceans 107 (C9), 3135. https://doi.org/10.1029/2000JC000294

Best, J., Simmons, S., Parsons, D., Oberg, K., Czuba, J., Malzon, C., 2010. A new methodology for the quantitative visualization of coherent flow structures in alluvial channels using multibeam echosounding (MBES). Geophys. Res. Lett. 37, L06405. https://doi.org/10.1029/2009GL041852

Bridge, J.S., 2003. Rivers and Floodplains; Forms, Processes, and Sedimentary Record. Blackwell Publ., Oxford, U.K., 600 pp.

Carling, P.A., Gölz, E., Orr, H.G., Radecki-Pawlik, A., 2000. The morphodynamics of fluvial sand dunes in the River Rhine, near Mainz, Germany. I. Sedimentology and morphology. Sedimentology 47, 227—252.

Cisneros, J., Best, J., van Dijk, T., de Almeida, R.P., Amsler, M., Boldt, J., et al., 2020. Dunes in the world's big rivers are characterized by low-angle lee-side slopes and a complex shape. Nature Geosci. 13, 156—162. https://doi.org/10.1038/s41561-019-0511-7

Davis, J.P., Walker, D.J., Townsend, M., Young, I.R., 2004. Wave-formed sediment ripples: Transient analysis of spectral development. J. Geophys. Res. 109, C07020. https://doi.org/10.1029/2004JC002307

Flemming, B.W., 1988. Zur Klassifikation subaquatischer, strömungstransversaler Transportkörper. Bochum Geol. Geotechn. Arb. 29, 44—47.

Guala, M., Heisel, M., Singh, A., Musa, M., Buscombe, D., Grams, P., 2020. A mixed length scale model for migrating fluvial bedforms. Geophys. Res. Lett. 47, 2019GL086625. https://doi.org/10.1029/2019GL086625

Harbor, D.J., 1998. Dynamics of bedforms in the lower Mississippi River. J. Sediment. Res. 68 (5), 750—762.

Hino, M., 1968. Equilibrium-range spectra of sand waves formed by flowing water. J. Fluid Mech. 34, 565—573. https://doi.org/10.1017/S0022112068002089

Hu, H., Wei, T., Yang, Zh, Christopher, R., Hackney, C.R., Parsons, D.R, 2018. Low-angle dunes in the Changjiang (Yangtze) Estuary: Flow and sediment dynamics under tidal influence. Estuar. Coast. Shelf Sci. 205, 110—122. https://doi.org/10.1016/j.ecss.2018.03.009

IMGW-PIB, 2020. www.pogodynka.pl. Online hydrological and meteorological database of the Institute of Meteorology and Wa-

ter Management — National Research Institute, Warsaw; Instytut Meteorologii i Gospodarki Wodnej — Państwowy Instytut Badawczy, Warszawa (accessed on 31 December 2020).

Julien, P.Y., Klaassen, G.J., 1995. Sand-dune geometry of large rivers during floods. J. Hydraul. Eng. 121 (9), 657—663. https://doi.org/10.1061/(ASCE)0733-429(1995)121:9(657)

Julien, P.Y., Klaassen, G.J., Ten Brinke, W.B.M., Wilbers, A.W.E., 2002. Case study: bed resistance of Rhine River during 1998 flood. J. Hydraul. Eng. 128 (12), 1042—1050. https://doi.org/10.1061/(ASCE)0733-9429(2002)128:12(1042)

Koop, L., van der Reijden, K.J., Mestdagh, S., Tom Ysebaert, T., Govers, L.L., Han Olff, H., Herman, P.M.J., Snellen, M., Dick, G., Simons, D.G., 2020. Measuring Centimeter-Scale Sand Ripples Using Multibeam Echosounder Backscatter Data from the Brown Bank Area of the Dutch Continental Shelf. Geosciences 10, 495. https://doi.org/10.3390/geosciences10120495

Lefebvre, A., Winter, C., 2016. Predicting bed form roughness: the influence of lee side angle. Geo-Mar. Lett. 36, 121—133. https://doi.org/10.1007/s00367-016-0436-8

Lisimenka, A., Kubicki, A., 2017. Estimation of dimensions and orientation of multiple riverine dune generations using spectral moments. Geo-Mar. Lett. 37, 59—74. https://doi.org/10.1007/s00367-016-0475-1

Lisimenka, A., Zwoliński, Z., Rudowski, S., 2015. The nature of the bed load transport in the mouth of the river to the non-tidal sea (the Vistula River, Poland), EGU General Assembly, Geophys. Res. Abst. 17 EGU2015-8955-1 (poster).

Lyons, P., Pouliquen, E., 2004. Advances in high-resolution seafloor characterization in support of high-frequency underwater acoustics studies: techniques and examples. Meas. Sci. Technol. 15, R59—R72. https://doi.org/10.1088/0957-0233/15/12/R01

Majewski, W., 2013. Sustainable development of the Lower Vistula. Meteorol. Hydrol. Water Manage. 1 (1), 33—37.

Majewski, W., 2018. Vistula River, its characteristics and management. Int. J. Hydrol. 2 (4), 493—496. https://doi.org/10.15406/ijh.2018.02.00116

Makowski, J., 1995. Setna rocznica wykonania Przekopu Wisły 1885-1995. IBW PAN, Gdańsk, 100 (in Polish).

Martin, R.L., Jerolmack, D.J., 2013. Origin of hysteresis in bed form response to unsteady flows. Water Resour. Res. 49, 1314—1333. https://doi.org/10.1002/wrcr.20093

Nelson, J.M., Logan, B.L., Kinzel, P.J., Shimizu, Y., Giri, S., Shreve, R.L., McLean, S.R., 2011. Bedform response to flow variability. Earth Surf. Process. Landforms 36, 1938—1947. https://doi.org/10.1002/esp.2212

Nikora, V., Sukhodolov, A., Rowinski, P.M., 1997. Statistical sand wave dynamics in one-directional water flows. J. Fluid Mech. 351, 17—39. https://doi.org/10.1017/S0022112097006708

Paarlberg, A.J., Dohmen-Janssen, C.M., Hulscher, S.J.M.H., Schielen, R., Termes, A.P.P., 2008. Modelling dynamic roughness in rivers during floods. In: Parsons, D.R., Garlan, T., Best, J.L. (Eds.), MARID 2008, 3rd international workshop on marine and river dune dynamics, 1-3 April 2008, Leeds, UK, 257—264.

Parsons, D.R., Best, J.L., Orfeo, O., Hardy, R.J., Kostaschuk, R., Lane, S.N, 2005. Morphology and flow fields of three-dimensional dunes, Rio Paraná, Argentina: Results from simultaneous multibeam echo sounding and acoustic Doppler current profiling. J. Geophys. Res. Earth. Surg. 110, F04S03. https://doi.org/10.1029/2004JF000231

Percival, D.B., Walden, A.T., 1993. Spectral analysis for physical applications. Cambridge University Press, Cambridge https://doi.org/10.1017/CBO9780511622762

Reesink, A.J.H., Parsons, D.R., Ashworth, P.J., Best, J.L., Hardy, R.J., Murphy, B.J., McLelland, S.J., Unsworth, C., 2018. The adaptation of dunes to changes in river flow. Earth-Sci. Rev. 185, 1065—1087. https://doi.org/10.1016/j.earscirev.2018.09.002

Rubin, D.M., McCulloch, D.S., 1980. Single and superimposed bedforms: a synthesis of San Francisco Bay and flume observations. Sediment. Geol. 26 (1—3), 207—231.

Rudowski, S., Edut, J., Wróblewski, R., Dworniczak, J., Lisimenka, A., Jereczek-Korzeniewska, K., Galer-Tatarowicz, K., 2017. Granulometry of bottom sediments of the Przekop Wisły canal. Bull. Maritime Inst. Gdańsk 32 (1), 14—20. https://doi.org/10.5604/12307424.1224050

Sambrook Smith, G.H., Best, J.L., Orfeo, O., Vardy, M.F., Zinger, J.A., 2013. Decimeter-scale in situ mapping of modern cross-bedded dune deposits using parametric echo sounding: A new method for linking river processes and their deposits. Gephys. Res. Lett. 40, 3883—3887. https://doi.org/10.1002/grl.50703

Szymański, E., 1897a. The regulation of the Vistula River mouth. Tech. Rev. 17, 270—274 (in Polish).

Szymański, E., 1897b. The regulation of the Vistula River mouth (continuation). Tech. Rev. 18, 285—289 (in Polish).

Ten Brinke, W.B.M., Wilbers, A.W.E., Wesseling, C., 1999. Dune growth, decay and migration rates during a large-magnitude flood at a sand and mixed sand—gravel bed in the Dutch Rhine river system. In: Smith, N.D., Rogers, J. (Eds.), Fluvial Sedimentology VI, 15—32. https://doi.org/10.1002/9781444304213.ch2

Van der Mark, C.F., Blom, A., 2007. A new and widely applicable tool for determining the geometric properties of bedforms. University of Twente, Enschede CE&M Research Report 2007R-003/WEM-002.

Van Rijn, L.C., 1984. Sediment transport. Part III: Bed forms and alluvial roughness. J. Hydr. Eng. 110 (12), 1733—1754.

Van Rijn, L.C., 1993. Principles of Sediment Transport in Rivers, Estuaries and Coastal Seas. AQUA Publications — I11, Amsterdam.

Venditti, J.G., Lin, C.-Y.M., Kazemi, M., 2016. Variability in bedform morphology and kinematics with transport stage. Sedimentology 63, 1017—1040. https://doi.org/10.1111/sed.12247

Warmink, J.J., Booij, M.J., Van der Klis, H., Hulscher, S.J.M.H., 2007. Uncertainty in water level predictions due to various calibrations. In: Proc. 1st International Conference on Adaptive & Integrated Water Management, CAIWA 2007, Basel, Switzerland, 1—18.

Warmink, J.J., Booij, M.J., Van der Klis, H., Hulscher, S.J.M.H., 2012. Quantification of uncertainty in design water levels due to uncertain bed form roughness in the Dutch river Waal. Hydrol. Process 27 (11), 1646—1663. https://doi.org/10.1002/hyp.9319

Warmink, J.J., Straatsma, M.W., Huthoff, F., Booij, M.J., Hulscher, S.J.M.H., 2013. Uncertainty of design water levels due to combined bed form and vegetation roughness in the Dutch River Waal. J. Flood Risk Manag. 6 (4), 302—318.

Warmink, J.J., 2014. Dune dynamics and roughness under gradually varying flood waves, comparing flume and field observations. Advances in Geosciences 39, 115—121. https://doi.org/10.5194/adgeo-39-115-2014

Wignall, P.B., Best, J.L., 2000. The Western Irish Namurian Basin reassessed. Basin Res. 12, 59—78.

Wilbers, A.W.E., Ten Brinke, W.B.M., 2003. The response of subaqueous dunes to floods in sand and gravel bed reaches of the Dutch Rhine. Sedimentology 50, 1013—1034. https://doi.org/10.1046/j.1365-3091.2003.00585.x

Wu, S., Jun Xu, Y., Wang, B., Cheng, H., 2021. Riverbed morphology of the Lowermost Mississippi River — Implications of leeside slope, flow resistance and bedload transport in a large alluvial river. Geomorphology 385, 107733. https://doi.org/10.1016/j.geomorph.2021.107733

Young, I., 1995. The determination of confidence limits associated with estimates of the spectral peak frequency. Ocean. Eng. 22, 669—689. https://doi.org/10.1016/0029-8018(95)00002-3